Materials Chemistry and Physics 138 (2013) 573–580

Contents lists available at SciVerse ScienceDirect

Materials Chemistry and Physics

journal homepage: www.elsevier.com/locate/matchemphys

Hot spots in photoreduced Au nanoparticles on DNA scaffolds potent for robust and high-sensitive surface-enhanced Raman scattering substrates

Hongwei Ma [a,b,1], Dongyue Lin [a,b,1], Honglin Liu [b,*], Liangbao Yang [b], Li Zhang [a,c], Jinhuai Liu [a,b,*]

[a] School of Life Science, Anhui University, Hefei 230039, PR China
[b] Institute of Intelligent Machines, Chinese Academy of Sciences, Hefei 230031, PR China
[c] Anhui Key Laboratory of Spin Electron and Nanomaterials (Cultivating Base), Suzhou College, Suzhou 234000, PR China

HIGHLIGHTS

- High-density Au NPs on DNA scaffolds were formed by in-situ photoreduction method.
- Interparticle gap of Au NPs on DNA can be finely controlled in the range of 1–3 nm
- The fabrication process was simple and just needs about 15 min
- The hybrid as SERS substrates produced empirical enhancement factors above 1×10^9.
- The results promised a rapid tool kit for nanofabrication of SERS substrates.

ARTICLE INFO

Article history:
Received 16 August 2012
Received in revised form
19 November 2012
Accepted 9 December 2012

Keywords:
Nanostructures
Composite materials
Raman spectroscopy and scattering
chemical synthesis

ABSTRACT

We demonstrate a one-step synthesis and controlled assembly of Au nanoparticles (NPs) on λ-DNA scaffolds by an in-situ photoreduction method. The interparticle gaps of the Au NPs attached on DNA can be fine regulated by controlling the *R* values (denoted as the ratio of Au(III) ions added per DNA base pair). At $R = 20$, the interparticle gap between two adjacent Au NPs on DNA is in the range of 1–3 nm *para*-aminothiophenol (PATP) as a Raman reporter is used to evaluate the surface-enhanced Raman scattering (SERS) performance of these DNA–Au hybrid substrates. Empirical enhancement factor above 1×10^9 is observed when the *R* value is in a fairly broad range of 10–60 under 785 nm excitation. At $R = 20$, this DNA–Au hybrid as SERS substrate can give a low detection limit of 0.5 nM of PATP, moreover, these substrates have a good reproducibility at different sites on a substrate, with a standard deviation of <15%. These results indicate that the photoreduced Au NPs on DNA scaffolds can be used as SERS-active substrates which exhibit high and reproducible SERS activity. This DNA–Au hybrid has potential applications in chemical and biological SERS analysis. Furthermore, the synthesis process is so simple and quick, which needs just only 15 min. Combined with the ability to make preformed scaffolds, the selective deposition of Au NPs on fixed DNA scaffolds will be an important addition to the rapidly growing nanofabrication tool kit for in-field SERS detection.

1. Introduction

The synthesis and assembly of noble metal NPs have received great attention due to their unique optical properties and wide range of applicability, especially in the field of SERS which is a powerful tool for chemical and biological analysis [1]. To date, giant SERS enhancements of around twelve orders of magnitude have been reported for aggregates of colloids, and single molecule-sensitive SERS has been already demonstrated by using "hot spots" in nanogaps between Ag or Au NPs [2]. However, the large electric field enhancements are located at a few random "hot spots" in the aggregates, making the systematic design of an efficient SERS substrate with a large active surface area difficult [3]. For example, an enhancement factor (EF) in the range from 10^3 to 10^5 was reported on the SERS activity of Au nanorods, spheres, tetrapods, cubes and dogbone structures using PATP as a Raman reporter [4], in contrast, the assembled Au nanosphere arrays with controlled

* Corresponding authors. Institute of Intelligent Machines, Chinese Academy of Sciences, Hefei 230031, PR China. Tel.: +86 551 65592385; fax: +86 551 65592420.
E-mail addresses: hlliu@iim.ac.cn (H. Liu), jhliu@iim.ac.cn (J. Liu).
[1] These authors contributed equally to this work.

0254-0584/$ – see front matter © 2012 Elsevier B.V. All rights reserved.
http://dx.doi.org/10.1016/j.matchemphys.2012.12.021

sub-10-nm gaps produced an EF of the order of 10^8 [5]. Hence, the SERS enhancement greatly depends on the NPs assembly. Two of the remaining challenges are how to increase the density of "hot spots" and further to control their uniform distribution over a macroscopically large area. In this context, accurately controlling the interparticle gap smaller than 10 nm is a major challenge to generate programmable assembly of NPs [6], which shows potential usefulness in high-sensitive SERS detection systems.

Several methods have been developed to control the assembly and the interparticle gap of two adjacent NPs [7–9]. For example, polymer single crystals [10], organic bridged ligands [11], DNA [12,13], and solid phase approaches [14] have been used to fabricate Au NPs dimer, trimer, tetramer, or large-scale assemblies. Considering all of these templates, DNA molecules are of special interest as the guide to assemble various materials [15] because of their unique periodic structures and programmable properties [16]. Particularly, DNA possesses a linear structure, large aspect ratio (length/diameter), well-defined sequences, and a variety of superhelix structures [17], and the negatively-charged phosphate groups of DNA have a strong affinity to bind the metal cations and positively-charged NPs [18–20]. The chemical reduction of metal-ions complexes with DNA has been investigated as a potential approach for creating conductive silver [21], gold [22], platinum [23], palladium [24], and copper [25] nanowires. In addition to the linear structure, large-scale DNA networks can also be fabricated by controlling DNA concentration [26]. A large-scale λ-DNA network on a mica surface was successfully fabricated through a self-assembly method [27]. Recently, our group reported a sunlight-induced formation of Ag–Au bimetallic nanostructures on DNA template for highly active SERS substrates to detect TNT and tumor marker [13], and we have also studied the sunlight-reduced Ag–DNA hybrid structure for ultratrace mercury analysis [12]. By the encouragement of these studies, we reasoned that it would be possible to control the interparticle gap through photoreduction of metal ions on DNA molecules under suitable conditions, and the in-situ photoreduction of NPs on DNA is friendly for SERS analysis because of the lack of any other reducing agents or protecting ligands.

Here we demonstrated a one-step synthesis and controlled assembly of Au NPs on DNA scaffolds by an in-situ photoreduction method. The photoreduction occurred by exposing the DNA–Au(III) solution to UV irradiation and the highly selective Au deposition could occur both on the DNA scaffolds in aqueous solution and that immobilized on a solid substrate. This method is high-yield and resulted in a new kind of Au–DNA hybrid nanostructures with a well-defined interparticle gap of ca. 1–3 nm between two adjacent Au NPs. The anchored DNA strands in these particles facilitated the formation of the nanogaps. This kind of nanogaps among the Au NPs resulted in the great amplification of the SERS signal, and produced a large EF of the order of 10^9. By controlling the DNA concentration, the size of Au NPs and the interparticle gap were tunable which allowed us to investigate the size and gap effects on the SERS signals. Moreover, the synthesis process was so simple and quick, which needs just about 15 min. Combined with the ability to make preformed scaffolds, the selective deposition of Au NPs on immobilized DNA will be an important addition to the rapidly growing nanofabrication tool kit for in-field SERS detection.

2. Experimental section

2.1. Materials

300 ng μl^{-1} λ-DNA containing 48,502 base pairs was purchased from Fermentas, and was extensively dialyzed in pure aqueous solution. Hydrogen tetrachloroaurate trihydrate ($HAuCl_4 \cdot 3H_2O$, 99.9%), trisodium citrate, and para-aminothiophenol (PATP) were A.R. grade and obtained from Shanghai Reagent Company. All solutions were prepared with double-distilled water.

2.2. Apparatus

UV–Vis spectra were collected with a spectral resolution of 0.5 nm on a TU-1901 model UV–Vis double beam spectrophotometer (Beijing Purkinje General Instrument Co., Ltd, China). Transmission electron microscopy (TEM) and high-resolution transmission electron microscopy (HRTEM) images were collected on a JEM-2100 electron microscope instrument (Japan Electron Co.). TEM and HRTEM samples were prepared by drop-coating the as-synthesized DNA–Au solution on carbon-coated copper grid, allowing the grid to stand for 2 min, and then removing the extra solution by the blotting paper. X-ray diffraction (XRD) analysis on a dry film of the DNA–Au solution on silicon substrate was carried out on a MAP18AHF instrument (Japan MAC Science Co.). Atomic force microscope (AFM) images were collected on a digital Nanoscope IIIa multimode system (DI, Santa Barbara, CA) with the tapping mode in air at room temperature with a Si cantilever. The force constant of the cantilever was 0.1–0.6 N m^{-1} with the scan rate at 1–2 Hz. Optical waveguide (OWG) absorption spectra were collected on the OWG installation built in our lab by Prof. Zhimei Qi in Institute of Electronics, Chinese Academy of Sciences, Beijing [28,29]. The experimental setup of OWG spectroscopy was illustrated in Fig. S1.

2.3. In-situ photoreduction of DNA–Au(III) complex in solution

In each sample, the final concentration of λ-DNA is 50 ng μl^{-1}. To form a DNA–Au(III) complex with the desired stoichiometry, the moles of base pairs were first determined on the basis of the 260 nm absorbance and considering for λ-DNA a molecular weight of 31.5×10^6 Da. Based on this calculation, DNA–Au(III) complexes of 1:1, 1:5, 1:10, 1:15, 1:20, 1:40, and 1:60 base pairs:Au(III) ratios were formed by adding the required amount of Au(III) in a 1 μl droplet, so to minimize dilution effects. The mixed solutions were placed directly under a 16 W UV lamp at a distance of 5 cm for a series of exposure times. The photoreduction was usually complete after 50 min.

2.4. Immobilization of DNA on OWG surface

Firstly, the glass surface was cleaned and hydroxylated by immersing in a piranha solution (a mixture of 98% H_2SO_4 and 30% H_2O_2, 7:3, v/v) at ~90 °C for ~1 h, followed by extensive rinsing with distilled water and drying under a stream of nitrogen (this rinsing and drying process should be performed in each of the following steps). Secondly, the hydroxylated substrate was immersing into a 10 mM 3-aminopropyltrimethoxysilane (APTS) ethanol solution for 2 h to form a 3-aminopropyl monolayer on its surface. The glass was rinsed with ethanol and heated at 110 °C for 1 h. Thirdly, the protonation of the amino groups was performed by immersing the substrate into 0.2 M HCl for 10 min.

λ-DNA (50 ng μl^{-1}) was immobilized on the OWG glass surface by a modification of the protocol developed in the literature [19]. The modified OWG glass was fitted onto the OWG stage (Fig. S1), λ-DNA was brought to a concentration of 50 ng μl^{-1} by diluting the stock solution in buffer system of 4-(2-hydroxyethyl)-1-piperazineethanesulfonic acid (HEPES) 40 mM, $MgCl_2$ 10 mM (pH 7.6), the solution poured in the sample cell and left to absorb for 5′. The solution containing DNA was carefully removed and the glass surface was washed by gently pouring 4–5 volumes of water.

2.5. In-situ photoreduction of DNA–Au(III) on OWG surface

λ-DNA (50 μg μl^{-1}) was immobilized on OWG glass by the method described above. After washing by water, the sample cell was filled again with approx. 1000 μl solution of $HAuCl_4$ at different concentrations, and the slide placed directly under a 16 W UV lamp at a distance of 5 cm. From the beginning of the UV exposure, the OWG absorption spectra were collected continuously. The acquisition time for each spectrum was 1 s.

2.6. SERS measurements

SERS measurements were conducted with a confocal microscopy Raman spectrometer (Thermo Fisher DXR Raman Microscope) equipped with a CCD detector and backscattered configuration using 50× objective lens. The SERS substrates were prepared at different stoichiometry of the DNA–Au(III) complex. The final concentration of DNA is 50 ng μl^{-1}, i.e. the concentration of DNA base pairs is 77 μM according the molecular weight of 31.5×10^6 Da and 48,502 base pairs in a λ-DNA molecule. Hence, for example, at $R = 20$, the final Au(III) is 1.54 mM. After the photoreduction, 1 ml of the as-prepared DNA–Au NPs hybrid solution was centrifuged at 8000 rpm for 10 min. The supernatant was discarded, and the pellet was re-dispersed as 10 μl. 10 μl of the as-prepared DNA–Au hybrid was dropped onto the surface of a silicon wafer and dried in air as the SERS substrate. The dried DNA–Au network film has a diameter of ca. 2 mm. Typically, a droplet of 5 μl PATP was added on DNA–Au network films. The samples were dried in air. Raman spectra were recorded with 785-nm laser with 10 mW power and 50× objective (1 μm^2 spot). The integral time is 5 s and aperture is 50 μm slit.

3. Results and discussion

3.1. In-situ photoreduced Au NPs on DNA in solution

On UV irradiation of an $HAuCl_4$ aqueous solution, Au microparticles are produced that immediately precipitate due to the absence of any stabilizers, and the rate of photoreduction is very slow, but can be significantly increased by adding an organic ligands. Earlier studies reported that Au(III) could react with DNA at pH = 5.6 to form a complex which was sensitive to mid-UV radiation [30], hence, we reasoned that it would be possible to control the interparticle gaps among Au NPs on DNA scaffolds through photoreduction process under suitable conditions. An intriguing challenge for fundamental research on NPs assembly is to achieve full control of the metal-ions coordination process, the subsequent nucleation, and the particle growth at the nanoscale level throughout the synthesis process. The photochemical method enables excellent spatial and temporal control for in-situ observations, avoids the use of harmful strong reducing agents, can be carried out at room temperature, moreover, the light can be simply turned off at the end of the synthesis.

A DNA–Au(III) solution is made by mixing 6 μg ml^{-1} DNA with different amounts of 2.43×10^{-2} M $HAuCl_4$ in water. The pure DNA solution had an absorption band at ~260 nm (curve a, Fig. S2), and on mixing with $HAuCl_4$ at $R = 20$ (R denoted as the number of $AuCl_4^-$ ion relative to DNA base pairs), a ~11% increase in the absorption band of DNA at 260 nm is observed. This hyperchromic effect is believed to be due to the electrostatic interaction between the positively-charged Au(III) cations and the negatively-charged phosphate groups of DNA. On UV irradiation of this mixed solution at 254 nm (intensity 16 W) for 5 min, the solution begun to turn pink with the appearance of an additional broad absorption band at 550 nm (curve b in Fig. 1A) due to the localized surface plasmon resonance (LSPR) of Au NPs. Interestingly, as the exposure time increased, the photoreduction process is accompanied by a significant blue-shift of the LSPR band (Fig. 1A). The initially arising of the LSPR band can be attributed to the nucleation and formation of Au NPs at higher $HAuCl_4$ concentration. As the exposure time increases, the increasing number of small Au NPs coexisted with the enlargement of Au NPs in the solution. We attribute the blue-shift to the formation of Au NPs with smaller dimension together with enlarged Au NPs. The LSPR band observed in Fig. 1A clearly indicated the formation of Au NPs in the 10–40 nm size range.

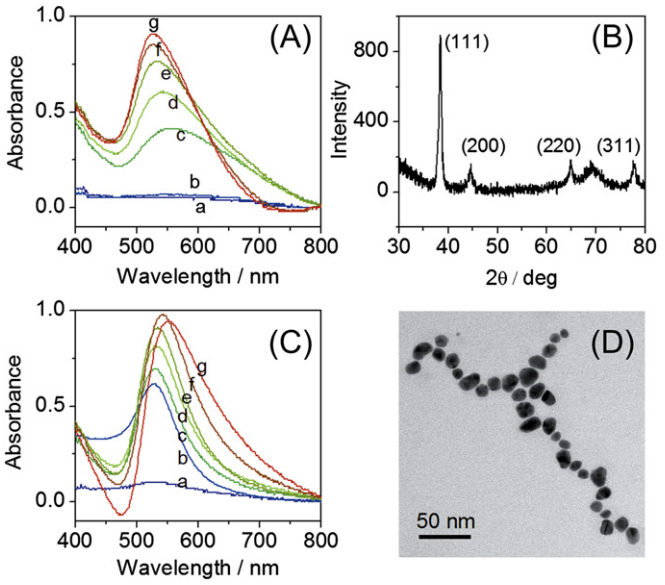

Fig. 1. Characterizations on UV irradiation-induced reduction of Au(III) on DNA scaffolds. (A) UV–Vis absorption spectra of the Au(III)–DNA solution ($R = 20$) with different exposure time under the UV irradiation: a, 0 min; b, 5 min; c, 10 min; d, 15 min; e, 20 min; f, 25 min; and g, 50 min. (B) XRD pattern recorded from a drop-coated film of DNA–Au(III) solution with an exposure time of 60 min. (C) UV–Vis absorption spectra of the Au(III)–DNA solution after 50 min exposure to UV irradiation at different R values: a, 1; b, 5; c, 10; d, 15, e, 20, f, 40; and g, 60. (D) TEM image of the photoreduced Au NPs on DNA scaffolds at $R = 20$. The conditions used in this system are as follows: [DNA] = 6 μg ml^{-1}, [$HAuCl_4$]/[base pair] = R (R denotes the ratio of $AuCl_4^-$ ion added per DNA base pair), and the wavelength of UV irradiation is 254 nm with a power of 16 W.

TEM observations clearly evidenced the photoreduced Au NPs had diameters of 19 ± 5 nm and arranged in a long linear pattern (Fig. 1D), which reflected the shape of DNA molecules. The XRD pattern recorded from a dry film on a silica substrate of the DNA–Au(III) solution after 50 min exposure to UV light is shown in Fig. 1B, and the (111), (200), (220) and (311) Bragg reflections are in good agreement with the face-centered cubic gold [13]. The mean sizes of the particles were 15 ± 6 nm according to Scherrer's equation ($d = k\lambda/\beta \cos\theta$), which was consistent with TEM observations. Moreover, monitoring the LSPR band at 525 nm as a function of the exposure time indicated that the LSPR band ceased to increase beyond 50 min of exposure, indicating completion of the reaction. For subsequent studies we fixed the exposure time to 50 min and varied R from 1 to 60 by changing the Au(III) content.

3.2. Relationship between the R values and the interparticle gap

Fig. 1C compared the LSPR bands of the formed Au NPs on DNA at different R values. The LSPR band increased as the R value increased from 1 to 40, and began to redshift and broaden when the R value was larger than 10. This broadening and redshift were indicative of larger size NPs with a broad size distribution, in other

words, the LSPR modes of two adjacent Au NPs started coupling when R is larger than 10. Extraordinary, the absorbance at $R = 60$ decreased. We speculated that as the concentration of Au(III) increased, the rate of reduction might be increased, and a larger R value might resulted in the aggregation or radial growth as guided by the DNA molecule. Hence, the absorbance of the LSPR peak decreased and a broad absorption band developed, as indicated by a redshift of the spectrum. Fig. 2 compared the size and interparticle gap of the formed Au NPs on DNA at $R = 20$ and 60. At $R = 20$, the average diameter of the photoreduced Au NPs on DNA scaffolds is 19 ± 5 nm (Fig. 2A), Fig. 2B–D showed the HRTEM observations on the interparticle gaps. More than 90% of the interparticle gaps were in the range of 2.1 ± 1.2 nm according to the Gauss fitting of the interparticle gap distribution (Fig. 2G). Furthermore, the relation between averaged NP diameter and gap size to the R values has been shown in Fig. S3. When the R values increase to 60, the adjacent Au NPs became close together, and the interparticle gap even disappeared as shown in Fig. 2E. The average diameter of the photoreduced Au NPs on DNA scaffolds increased to 55 ± 12 nm (Fig. 2F and Fig. S3E).

It is mysterious that the size and interparticle gap of the photoreduced Au NPs could be controlled by the DNA structures. When the R value is small, the particle size is limited by the DNA structure, and the interparticle gap became smaller along with the increase of the R values. One possible explanation for this phenomenon may be the physical contact of the polymer chain with the surface of NPs, which prevents its further growth and controls its final gap [20]. When the R value became larger, the formation of the larger Au NPs could induced the breakage of the DNA structures, and sequentially induced the aggregation of Au NPs as observed in the literature. When the R value became large enough, a network of DNA–Au nanowires could be formed (Fig. S4). Interestingly, at $R = 100$, the horizontal diameter of the Au nanowire is about 50–70 nm, which is similar with that of Au NPs formed at $R = 60$ in Fig. 2F. Increasing the Au(III) load, the nucleation became more easier and frequent. We speculated that the growth process is self-limiting, a factor which would be consistent with the templating and catalytic effect provided by the DNA [19]. Therefore, this provides a possible way for us to precise control the interparticle gap of Au NPs. By changing the R value, a highly-sensitive SERS substrate might be synthesized under suitable conditions, this will be discussed in detailed later.

3.3. The photoreduction and assembly process of Au NPs on fixed DNA scaffolds

The discussions above were based on the TEM observations on dry films of DNA–Au hybrid structure on the carbon-coated copper grids. The pattern and the interparticle gap of the in-situ photoreduced Au NPs on DNA in solution might be altered during the preparation of the TEM samples. To validate the interference that the interparticle gap could be fine regulated by changing the R values, we try to fix the DNA molecules on a flat surface and monitoring the

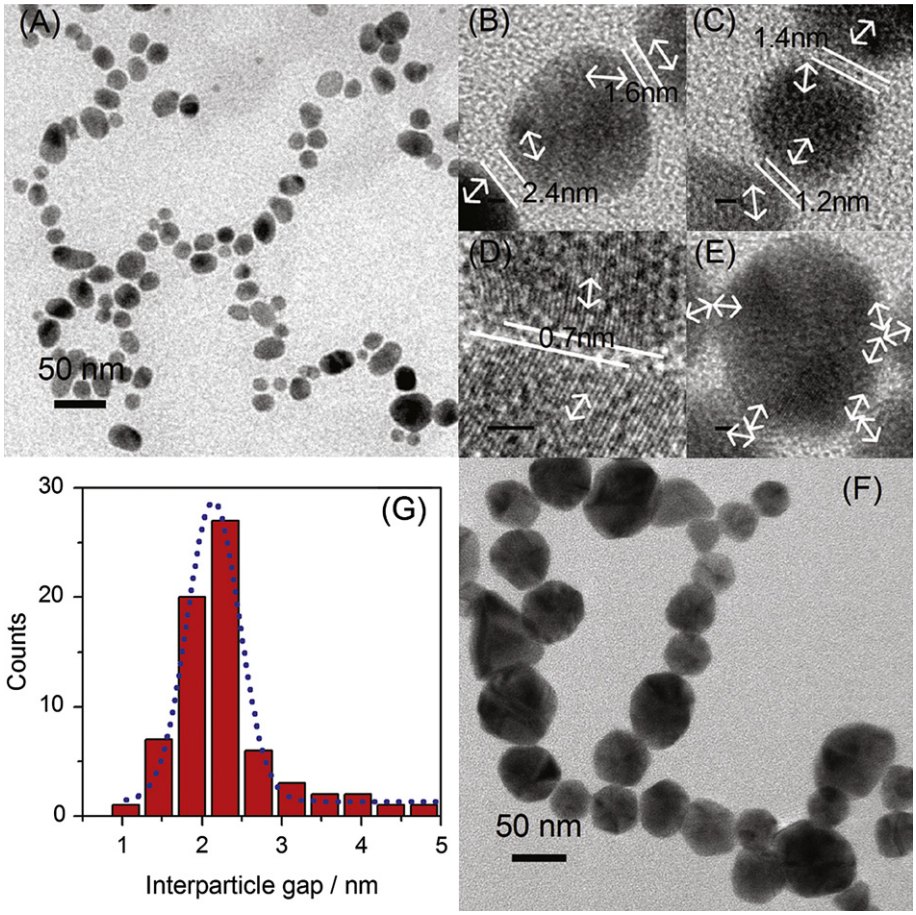

Fig. 2. Size and interparticle gap distribution of the UV irradiation-reduced Au NPs on DNA scaffolds. (A) TEM and (B, C, D) HRTEM images of the UV irradiation-reduced Au NPs on DNA scaffolds at $R = 20$. (E) TEM and (F) HRTEM images of the UV irradiation-reduced Au NPs on DNA scaffolds at $R = 60$. Those white two-way arrows on HRTEM images indicated the lattice directions of the Au NPs, and all black scale bars on HRTEM images represent 2 nm. (G) Histogram of the corresponding interparticle gap distribution shown in the TEM image A. The blue dot line represented the Gauss fitting of the interparticle gap distribution. (For interpretation of the references to color in this figure legend, the reader is referred to the web version of this article.)

photoreduction and assembly of Au NPs on the fixed DNA scaffolds. Fortunately, OWG spectroscopy could be used to real-time monitor the in-situ photoreduction and assembly process of Au NPs on DNA scaffolds. OWG spectroscopy is a rather new and powerful technique for surface monitoring. The technique takes advantage of the evanescent field, which penetrates less than a wavelength out of the waveguide surface, to selectively respond to the adsorption of immobilized chemical or biological molecules over a given spectral bandwidth. The acquisition time for each spectrum was as short as 1 s, hence, OWG spectroscopy could accurately monitor the UV irradiation-induced reduction process of Au NPs on DNA scaffolds.

Here, λ-DNA is stretched, aligned, and immobilized on an OWG glass surface by the molecular combing method (Fig. 3B) [19]. By adding different concentrations of $HAuCl_4$ solution into the sample cell (Fig. S1), Au(III) could form complexes with the fixed DNA molecules on OWG glass surface, we used the OWG spectroscopy to monitor the real-time photoreduction and dynamic assembly process. Fig. 3A showed the real-time OWG absorption spectra monitoring UV irradiation-induced formation of Au NPs on fixed DNA scaffolds at $R = 5$. Under this low concentration of Au(III), the UV irradiation resulted in the appearance of an absorbance peak centered at ca. 490 nm, which

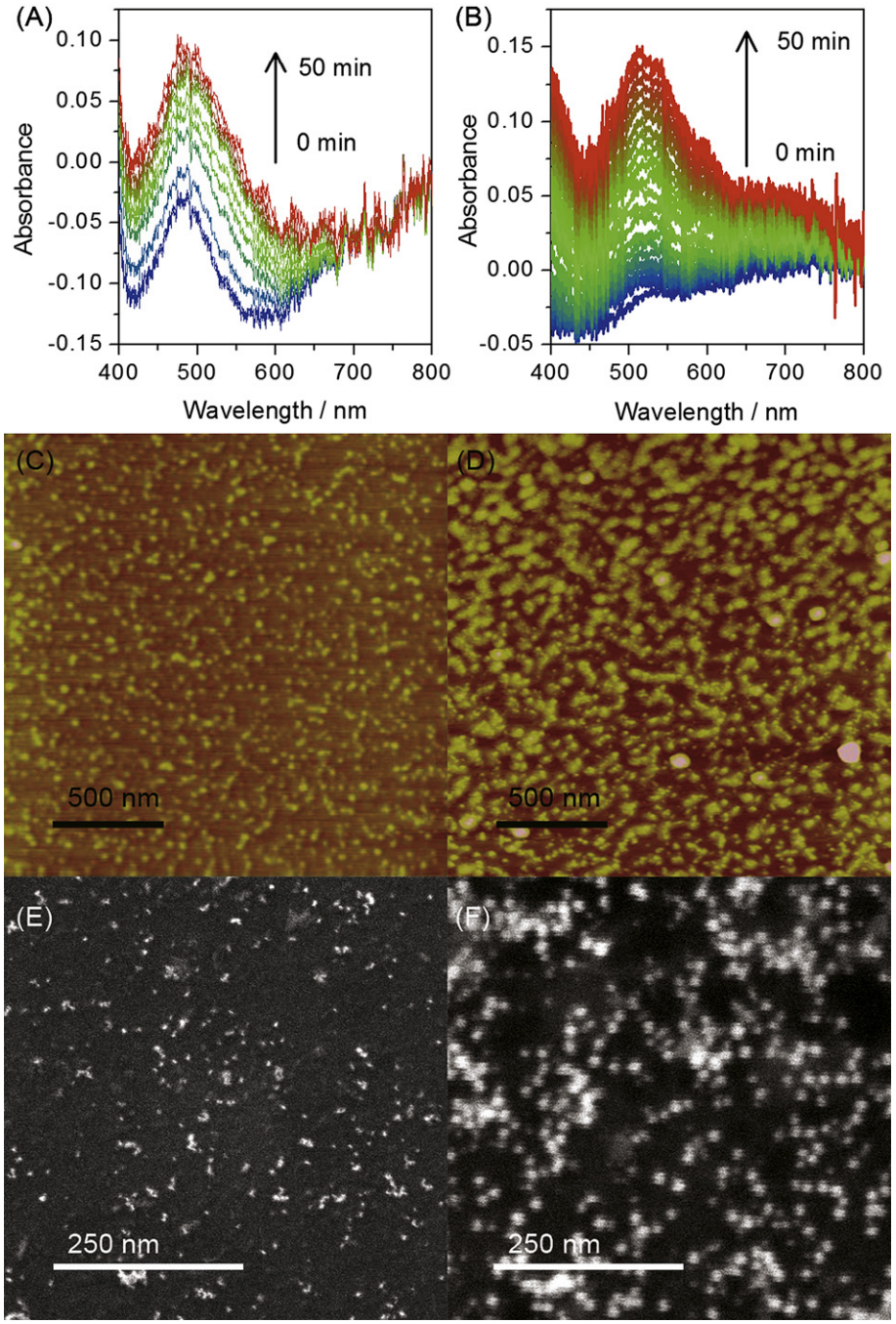

Fig. 3. (A and B) The real-time OWG absorption spectra monitoring the photoreduction and assembly process of Au NPs on the fixed DNA scaffolds at $R = 5$ and $R = 20$, respectively. (C and D) tapping mode AFM observations on the photoreduced Au NPs on DNA scaffolds at $R = 5$ and $R = 20$, respectively. (E and F) SEM observations on the photoreduced Au NPs on DNA scaffolds at $R = 5$ and $R = 20$, respectively. In these experiments, [DNA] = 50 ng μl^{-1}, and the R values were evaluated on the basis of this DNA concentration, although it was possible that not all the DNA molecules adsorbed on the OWG surface.

could be attributable to the LSPR peak of the small Au nanoclusters. When we prolonged the reaction time, there was not a redshift of this LSPR or the appearance of new peaks at longer wavelengths. This result indicated that all Au(III) ions should be reduced and assembled on the fixed DNA. The size of NPs in Fig. 3C might be overestimated in AFM image due to low special resolution in lateral direction. Nevertheless, both the AFM and SEM observations (Fig. 3C and E) evidenced that the photoreduced particles were small and the interparticle gap was big due to the lack of Au(III) contents in this system.

Nevertheless, as shown in Fig. 3B, the real-time OWG absorption spectroscopy was used to monitor the UV irradiation-induced formation of Au NPs on fixed DNA scaffolds at $R = 20$. Under this high concentration of Au(III), the UV irradiation resulted in the appearance of an absorbance peak centered at ca. 525 nm, which could be attributable to the LSPR peak of the relatively larger Au NPs. When we prolonged the reaction time, the appearance of a shoulder peak at longer wavelengths (630–750 nm) was attributed to the coupling or aggregating of Au NPs on the fixed DNA scaffolds [31]. After 50 min of exposing to UV irradiation, the intensity of the OWG absorbance became stable. The results also indicated that the interaction is stably enough to complete the spectra collection. In Fig. 3D and F, the AFM and SEM observations showed the large Au NPs and the small interparticle gap. These observations were in good agreement with the results of UV–Vis spectroscopy and TEM images. In other words, the photoreduced Au NPs can occur both on DNA in solution and on the fixed DNA scaffolds on OWG surface and the interparticle gap could be controlled by changing the R values. Moreover, we performed a line map measurement showing where the SERS spectra are obtained from and how the SERS intensity varies across the sample (Fig. S5). The diameter of the laser focal spot is about 1 μm, and the data interval is 1 μm. It showed that the SERS signal at every point can be collected within a range of −10 μm to 10 μm. These results indicated that the hybrid substrate is stable.

3.4. SERS studies of the photoreduced DNA–Au hybrid

As mentioned earlier, since the interparticle gap of the photoreduced Au NPs on DNA could be fine regulated, the as-prepared DNA–Au hybrid may promise a great future in the SERS measurements. Here, the SERS performance of DNA–Au hybrids was quantitatively evaluated using a nonresonant molecule, PATP, as the analyte. PATP is ideal for quantification because it forms self-assembled monolayers with a known packing density on Au surfaces by forming an Au–S bond [31].

Fig. 4 showed the SERS spectra obtained from a series of DNA–Au hybrid samples at different R values treated in 10 nM PATP with 780 nm excitation. The Raman bands at about 1580, 1441, 1391, 1185, 1140, and 1074 cm^{-1} can be attributed to PATP and agree well with the literature data [12]. It can be found from Fig. 4 that the SERS signals of PATP first increased and then decreased as the R values increased from 5 to 60, which reached the strongest strength at $R = 20$. Interestingly, the DNA molecules are not detected in the SERS. Many studies have shown that spectral quality and reproducibility can be severely limited by large variations in molecular conformation and/or packing density of the DNA, and the sensitive and reliable acquisition of SERS spectra from DNA remains a significant challenge [32]. Regardless of the DNA composition, sequence, and hybridization state, the SERS spectra of the DNA exhibit almost identical spectral features dominated by adenine [32], whereas cytosine and thymine did not show detectable signal [33]. By the use of DNA-reduced Ag, Au, or Au/Ag core–shell structures as the SERS substrate, the DNA–metal hybrid only shows two significant broadened bands at 1350 and 1650 cm^{-1} [13]. These

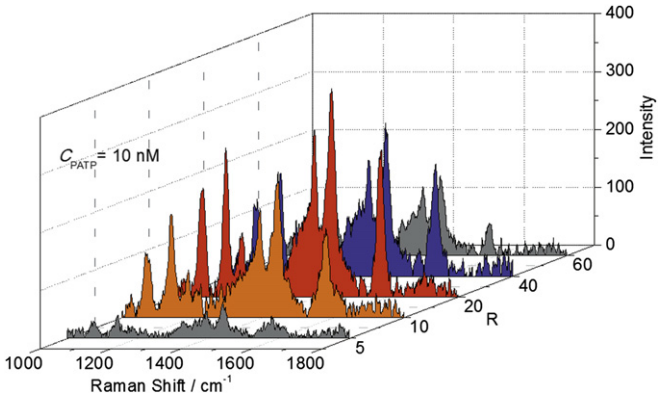

Fig. 4. SERS spectra of 10 nM PATP molecules obtained from the UV irradiation-reduced Au NPs on DNA scaffolds at different R values.

two bands did not affect the SERS signal collection of the targeted analytes.

The SERS band at 1441 cm^{-1} assigned to the combination of C–C stretching and C–H bending vibration was used for the estimation of the enhancement factor (EF). The EF for DNA–Au hybrid substrates was calculated according to Eq. (1) [34].

$$\mathrm{EF} = \frac{I_{\mathrm{SERS}}/N_{\mathrm{SERS}}}{I_{\mathrm{bulk}}/N_{\mathrm{bulk}}} \tag{1}$$

where I_{SERS} and I_{bulk} represent the peak intensities at 1441 cm^{-1} collected from the DNA–Au hybrid substrate and the solid powder, respectively. N_{SERS} is the average number of adsorbed molecules in the scattering volume for the SERS measurements. N_{bulk} is the molecule number of the neat PATP in the laser illumination volume. We employed 785 nm laser and focused through objective lens (50×, Numerical Aperture (NA) = 0.5) to reduce instrumental noise. Assuming that the excitation volume as a cylinder, the diameter (d) and the height (h) were determined by the following equations:

$$d = \frac{1.22\lambda_{\mathrm{laser}}}{\mathrm{NA}} \tag{2}$$

$$h = \frac{2.2n\lambda_{\mathrm{laser}}}{\pi(\mathrm{NA})^2} \tag{3}$$

where n is the refractive index of PATP ($n \approx 1.6$) [35]. Table 1 shows the calculated EF values for the prepared DNA–Au hybrid substrates.

According to the data in Table 1, empirical EFs above 1×10^9 are observed when the R values were in a fairly broad range of 10–60 with 785 nm excitation. We clearly know that it is difficult to calculate an accurate enhancement factor. For comparison, it is best to compare the enhancement of the similar Au NPs without DNA. Fortunately, PATP as a Raman reporter has been widely used to evaluate the SERS performance of various nanomaterials. An EF in

Table 1
Enhancement factors for PATP (10 nM) using different colloids.

Colloids	EF
$R = 5$	6.0×10^8
$R = 10$	2.3×10^9
$R = 20$	3.5×10^9
$R = 40$	2.4×10^9
$R = 60$	1.3×10^9

the range from 10^3 to 10^5 was reported on the SERS activity of Au nanorods, spheres, tetrapods, cubes and dogbone structures [4,36]. The SERS activity of aggregated and non-aggregated Au nanorod films gave an enhancement of the order of 10^5 and 10^4 respectively [37,38]. It can be seen that the assembly of Au NPs on DNA greatly increases the SERS enhancement. Similarly, an EF of the order of 10^8 was demonstrated by the use of Au nanosphere arrays with controlled sub-10-nm gaps [5]. And the empirical EFs of our DNA–Au hybrid are nearly one-order of magnitude higher than the Au nanosphere arrays.

It is very essential to explain the excellent performance of the as-synthesized DNA–Au hybrid, and to explore why the DNA–Au hybrid with different R values produced dissimilar SERS performance (Fig. 4). According to the above studies, the different size of the interparticle gap should be responsible for the difference in SERS performance. The SERS-active substrate supported on the DNA chain is composed of close-packed Au NPs, which leads to a large total surface area and may form a large number of hot spots. When excited by incident light, the hot spots can contribute to larger SERS enhancement. When the R values increased from 5 to 60, the size of Au NPs became large. In the very beginning, the size might mainly contribute to the increase in enhancement of the SERS signal. Nevertheless, when the interparticle gap became less than 10 nm, the hotspot effect should become the main factor that affect the enhancement of the SERS signal. At $R = 20$, the interparticle gap of the photoreduced Au NPs on DNA scaffolds resulted in the largest enhancement of the SERS signal. When the R values further increased, the adjacent Au NPs attached on DNA chain became close together, and even made the interparticle gap disappear. This should be why the enhancement of the SERS signals became smaller at $R > 20$.

To evaluate the sensitivity and reproducibility of the DNA–Au hybrid substrates, parallel experiments using different batches of the photoreduced Au NPs on DNA scaffolds were carried out. 5 μL of the probe molecules with different concentrations were deposited on the SERS-active substrate of DNA–Au hybrid ($R = 20$), and then the samples were dried in air. PATP can form a close-packed and orientated spontaneously on Au surface based upon the strong covalent bonding between the thiol group and the Au substrate. As shown in Fig. 5A, the vibration of C–S (1076 cm^{-1}) and C–C (1076, 1184, 1441, and 1578 cm^{-1}) will be enhanced greatly. As the concentration of PATP increases, the SERS Stokes' intensities of the C–S and C–C bonds of PATP significantly increase (Fig. 5A). Although the fingerprint peaks of the SERS signal arose from 0.1 nM PATP could be distinguished, according to the criteria of the signal-to-noise = 3, the DNA–Au hybrid as SERS substrate can give a low detection limit of 0.5 nM. In addition, the SERS spectra of PATP on the DNA–Au hybrid substrates were reproducible at different sites on a substrate, with a standard deviation of <15%. These results indicated that the photoreduced Au NPs on DNA scaffolds can be used as SERS substrates which exhibit high SERS activity and reproducibility.

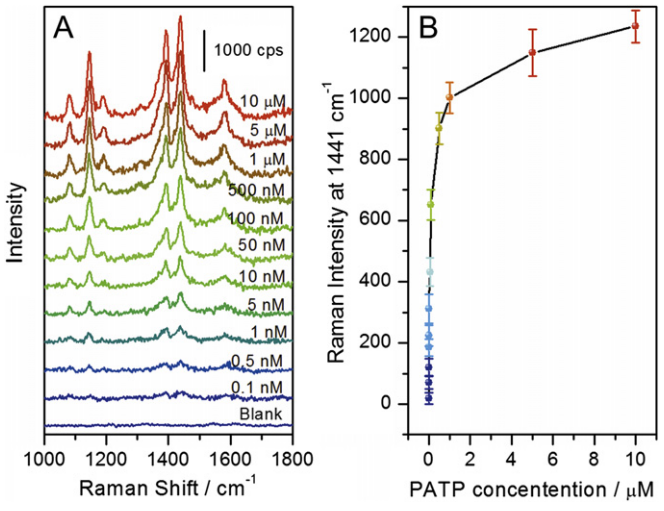

Fig. 5. (A) SERS spectra of PATP molecules at different concentrations obtained from the photoreduced Au NPs on DNA scaffolds at $R = 20$. (B) Plot demonstrating how Raman intensity at 1441 cm^{-1} changes upon addition of 5 μl PATP at different concentrations onto the DNA–Au hybrid substrate at $R = 20$.

4. Conclusions

In summary, a simple and one-step method has been used to synthesize DNA–Au hybrid by the photoreduction. The interparticle gap of the photoreduced Au NPs on DNA scaffolds was mainly associated with the molar ratio of Au(III) ions to DNA base pairs. DNA as an effective template and the reducing agent plays an important role in controlling the shape and the size of Au NPs. These novel nanostructures acting as SERS-active substrates were demonstrated, and exhibited great enhancement on SERS signals. The enhancement factor is dependent on the interparticle gap of two adjacent Au NPs attached on DNA. It is possible to achieve larger field enhancement factors by adjusting the ratio between the DNA base pairs and the metal ions. The gap of two adjacent Au NPs can be fine regulated to 1–3 nm under suitable conditions. Extremely intense local electromagnetic fields can be generated in this case. This kind of DNA–Au hybrid acting as a SERS substrate could have potential applications in chemical and biological analysis. Moreover, the synthesis process was so simple and quick, which needs just about 15 min. Combined with the ability to make preformed scaffolds, the selective deposition of Au NPs on immobilized DNA will be an important addition to the rapidly growing nanofabrication tool kit for in-field SERS detection.

Acknowledgments

This work was supported by the National Basic Research Program of China (2011CB933700), the National Instrumentation Program of China (2011YQ0301241001 and 2011YQ0301241101), and the National Natural Science Foundation of China (21271136).

Appendix A. Supplementary data

Supplementary data associated with this article can be found, in the online version, at http://dx.doi.org/10.1016/j.matchemphys.2012.12.021.

References

[1] J.P. Camden, J.A. Dieringer, J. Zhao, R.P. Van Duyne, Acc. Chem. Res. 41 (2008) 1653.
[2] K. Kneipp, H. Kneipp, J. Kneipp, Acc. Chem. Res. 39 (2006) 443.
[3] Y. Fang, N.H. Seong, D.D. Dlott, Science 321 (2008) 388.
[4] X. Hu, T. Wang, L. Wang, S. Dong, J. Phys. Chem. C 111 (2007) 6962.
[5] H. Wang, C.S. Levin, N.J. Halas, J. Am. Chem. Soc. 127 (2005) 14992.
[6] N.H. Kim, S.J. Lee, M. Moskovits, Adv. Mater. 23 (2011) 4152.
[7] J.S. Shumaker-Parry, R. Sardar, T.B. Heap, J. Am. Chem. Soc. 129 (2007) 5356.
[8] N. Ji, W. Ruan, Z. Li, C. Wang, Z. Yang, B. Zhao, J. Raman Spectrosc. (2012). http://dx.doi.org/10.1002/jrs.4132.
[9] R. Que, M. Shao, S. Zhuo, C. Wen, S. Wang, S.T. Lee, Adv. Funct. Mater. 21 (2011) 3337.
[10] G. Bunte, J. Hurttlen, H. Pontius, K. Hartlieb, H. Krause, Anal. Chim. Acta 591 (2007) 49.
[11] L.C. Brousseau, J.P. Novak, S.M. Marinakos, D.L. Feldheim, Adv. Mater. 11 (1999) 447.
[12] H.L. Liu, L.B. Yang, H.W. Ma, Z.M. Qi, J.H. Liu, Chem. Commun. 47 (2011) 9360.
[13] L.B. Yang, G.Y. Chen, J. Wang, T.T. Wang, M.Q. Li, J.H. Liu, J. Mater. Chem. 19 (2009) 6849.

[14] K.M. Sung, D.W. Mosley, B.R. Peelle, S.G. Zhang, J.M. Jacobson, J. Am. Chem. Soc. 126 (2004) 5064.
[15] F.A. Aldaye, A.L. Palmer, H.F. Sleiman, Science 321 (2008) 1795.
[16] F.A. Aldaye, H.F. Sleiman, J. Am. Chem. Soc. 129 (2007) 4130.
[17] H. Yang, A.Z. Rys, C.K. McLaughlin, H.F. Sleiman, Angew. Chem. Int. Ed. 48 (2009) 9919.
[18] H. Arakawa, J.F. Neault, H.A. Tajmir-Riahi, Biophys. J. 81 (2001) 1580.
[19] L. Berti, A. Alessandrini, P. Facci, J. Am. Chem. Soc. 127 (2005) 11216.
[20] J.T. Petty, J. Zheng, N.V. Hud, R.M. Dickson, J. Am. Chem. Soc. 126 (2004) 5207.
[21] E. Braun, Y. Eichen, U. Sivan, G. Ben-Yoseph, Nature 391 (1998) 775.
[22] R.F. Saraf, S. Kundu, V. Maheshwari, Langmuir 24 (2008) 551.
[23] M. Mertig, R. Seidel, L.C. Ciacchi, M. Weigel, W. Pompe, J. Phys. Chem. B 108 (2004) 10801.
[24] J. Richter, R. Seidel, R. Kirsch, M. Mertig, W. Pompe, J. Plaschke, H.K. Schackert, Adv. Mater. 12 (2000) 507.
[25] A.T. Woolley, C.F. Monson, Nano. Lett. 3 (2003) 359.
[26] A.G. Wu, Z. Li, H.L. Zhou, J.P. Zheng, E.K. Wang, Analyst 127 (2002) 585.
[27] G. Wei, L. Wang, Z.G. Liu, Y.H. Song, L.L. Sun, T. Yang, Z.A. Li, J. Phys. Chem. B 109 (2005) 23941.
[28] Z.M. Qi, N. Matsuda, J.H. Santos, Opt. Lett. 27 (2002) 689.
[29] Z.M. Qi, N. Matsuda, T. Yoshida, H. Asano, A. Takatsu, K. Kato, Opt. Lett. 27 (2002) 2001.
[30] R.J. Wilkins, Photosensitization of DNA by gold, Nucleic Acids Res. 5 (1978) 3731.
[31] N. Mohri, S. Matsushita, M. Inoue, K. Yoshikawa, Langmuir 14 (1998) 2343.
[32] A. Barhoumi, D.M. Zhang, F. Tam, N.J. Halas, J. Am. Chem. Soc. 130 (2008) 5523.
[33] B. Pignataro, A. De Bonis, G. Compagnini, P. Sassi, R.S. Cataliotti, J. Chem. Phys. 113 (2000) 5947–5953.
[34] E. Galopin, J. Barbillat, Y. Coffinier, S. Szunerits, G. Patriarche, R. Boukherroub, ACS Appl. Mater. Inter. 7 (2009) 1396.
[35] R. Liu, B. Liu, G. Guan, C. Jiang, Z. Zhang, Chem. Commun. 48 (2012) 9421.
[36] K. Kim, J.K. Yoon, J. Phys. Chem. B 109 (2005) 20731.
[37] Y. Wang, S. Guo, H. Chen, E. Wang, J. Colloid Interf. Sci. 318 (2008) 82.
[38] S.L. Smitha, K.G. Gopchandran, T.R. Ravindran, V.S. Prasad, Nanotechnology 22 (2011) 265705.